The Indian Ocean Sea Surface Temperature Warming Simulated by CMIP5 Models during the Twentieth Century: Competing Forcing Roles of GHGs and Anthropogenic Aerosols

LU DONG

State Key Laboratory of Numerical Modeling for Atmospheric Sciences and Geophysical Fluid Dynamics, Institute of Atmospheric Physics, Chinese Academy of Sciences, and University of Chinese Academy of Sciences, Beijing, China

TIANJUN ZHOU

State Key Laboratory of Numerical Modeling for Atmospheric Sciences and Geophysical Fluid Dynamics, Institute of Atmospheric Physics, and Climate Change Research Center, Chinese Academy of Sciences, Beijing, China

(Manuscript received 3 July 2013, in final form 16 January 2014)

ABSTRACT

The Indian Ocean exhibits a robust basinwide sea surface temperature (SST) warming during the twentieth century that has affected the hydrological cycle, atmospheric circulation, and global climate change. The competing roles of greenhouse gases (GHGs) and anthropogenic aerosols (AAs) with regard to the Indian Ocean warming are investigated by using 17 models from phase 5 of the Coupled Model Intercomparison Project (CMIP5). The increasing GHGs are considered to be one reason for the warming. Here model evidence is provided that the emission of AAs has slowed down the warming rate. With AAs, the warming trend has been slowed down by 0.34 K century^{-1}. However, the cooling effect is weakened when only the direct aerosol effect is considered. GHGs and AAs have competed with each other in forming the basinwide warming pattern as well as the equatorial east–west dipole warming pattern. Both the basinwide warming effect of GHGs and the cooling effect of AAs, mainly through indirect aerosol effect, are established through atmospheric processes via radiative and turbulent fluxes. The positive contributions of surface latent heat flux from atmosphere and surface longwave radiation due to GHGs forcing dominate the basinwide warming, while the reductions of surface shortwave radiation, surface longwave radiation, and latent heat flux from atmosphere associated with AAs induce the basinwide cooling. The positive Indian Ocean dipole warming pattern is seen in association with the surface easterly wind anomaly during 1870–2005 along the equator, which is produced by the increase of GHGs but weakened by AAs via direct aerosol effects.

1. Introduction

During the twentieth century, the basinwide Indian Ocean sea surface temperature (SST) warming was the strongest and most robust warming signal around the global oceans, especially since the 1950s (Lau and Weng 1999; Hoerling et al. 2004; Du and Xie 2008), mainly due to the stronger wind stress curl and subtropical gyre in Indian Ocean (Cai et al. 2007; Alory et al. 2007). The warming is not confined to the surface, but also penetrates down to around 200 m (Cai et al. 2007). The Indian Ocean SST warming is related to the decrease in African Sahel rainfall (Giannini et al. 2003) and also influences the Northern Hemisphere midlatitude circulation (Lu et al. 2004; Hoerling et al. 2004), North Atlantic weather regimes (Sanchez-Gomez et al. 2008), Maritime Continent and Australian rainfall (Chang and Li 2000; Ashok et al. 2003), the southwest monsoon circulation in South Asian monsoon regime (Krishnan et al. 2006), the North Pacific storm track (Chu et al. 2013), the westward extension of the western Pacific subtropical high, and the east–west expansion of the South Asian high (Zhou et al. 2009), as well as remote forcing of ENSO (Lau et al. 2006; Hong et al. 2010).

Denotes Open Access content.

Corresponding author address: Tianjun Zhou, LASG, Institute of Atmospheric Physics, Chinese Academy of Sciences, P.O. Box 9804, Beijing 100029, China.
E-mail: zhoutj@lasg.iap.ac.cn

DOI: 10.1175/JCLI-D-13-00396.1

There are many studies on the mechanisms responsible for the SST warming under greenhouse gas (GHG) forcing. The increasing GHGs responsible for the warming of the global ocean were first recognized by Revelle et al. (1965). The warming trend over the tropical Indian Ocean can be reproduced by coupled general circulation models (CGCMs) forced by increased GHG concentrations (Barnett et al. 2005; Pierce et al. 2006; Knutson et al. 2006; Alory et al. 2007). However, the mechanism for the Indian Ocean response to the GHG forcing remains an open question in climate models (Du and Xie 2008). Some studies suggested that the SST warming is directly triggered by atmospheric processes. The warming is induced by the increase in downward longwave radiation due to GHGs, and then amplified by the water vapor feedback and atmospheric adjustment in climate models (Du and Xie 2008). Other studies suggest that this SST change is linked to the changes in heat transport by the ocean. For example, Indian Ocean basinwide warming is associated with the ocean wave-induced thermocline change (Li et al. 2003) or a decrease in the upwelling that is related to a slowdown of the wind-driven Ekman pumping (Alory and Meyers 2009). Both atmospheric and oceanic processes have contributions in some modeling studies. The ocean temperature advection is regarded as the dominant process for the increase of the northern Indian Ocean heat content, while surface heat fluxes prevail in other areas of the Indian Ocean basin (Barnett et al. 2005).

In addition to GHGs, aerosols probably exert the second largest anthropogenic radiative forcing of the climate (Solomon et al. 2007, 200–205; Mitchell et al. 1995), especially the effects of black carbon, sulfate aerosols, and organic carbon. The inclusion of aerosol forcing can improve the simulation of global mean temperature over the last few decades in climate system models (Mitchell et al. 1995). Aerosols can have a large effect on the global and regional climate change (e.g., Ming et al. 2011; Ramanathan and Carmichael 2008). Despite the aerosol-induced surface heat flux change being constrained to the Northern Hemisphere, increasing aerosols may cause reductions of heat content in both hemispheres (Cai et al. 2006). The Northern Hemisphere is cooled via a reduction in surface heat flux, whereas the Southern Hemisphere is cooled via hemispheric heat transport, acting via a strengthening of the global conveyor to increase the warming rate in the subtropics that takes heat out of the off-equatorial region, generating a cooling (Cai et al. 2007). The emission of anthropogenic aerosols (AAs) can influence ocean circulation (Collier et al. 2013; Cowan and Cai 2013), monsoon circulations (Song et al. 2014), and the subtropical jet in the Southern Hemisphere (Rotstayn et al. 2013), and is associated with the fast warming of the southern midlatitude oceans (Cai et al. 2010). The aerosol forcing is also regarded as one driver of the Atlantic multidecadal oscillation (AMO) (Booth et al. 2012), and it weakens the hydrological cycle over northern high latitudes with a southward shift of the intertropical convergence zone (ITCZ) (Chen et al. 2010). In explaining the ITCZ shift the indirect aerosol effects have been emphasized in Chang et al. (2011) and Chiang et al. (2013). For the Indian Ocean, the potential roles of AAs in the temperature trends of the subthermocline (Cai et al. 2007; Cowan et al. 2013), as well as the decadal variability of sea level and thermocline depth (Trenary and Han 2013), have been pointed out. There are suggestions from decadal predictions that Indian Ocean SST simulation ability also arises from AA emission changes, although volcanic aerosols play a greater role in simulating its interannual variability (Guemas et al. 2013).

The competition between GHGs and AAs forcing has been revealed in other contexts. For example, Mitchell et al. (1995) predicted a future global mean warming of 0.3 K decade^{-1} for GHG forcing alone, but 0.2 K decade^{-1} with sulfate aerosols included by using a climate model of the Hadley Centre. For global ocean volume mean temperature and sea level change, AAs still appear to play a major role in offsetting the rising effects from the increased well-mixed GHGs (Delworth et al. 2005). In addition, increasing AAs strengthen the North Atlantic thermohaline circulation, also competing against the effects of increasing GHGs in the late twentieth century (Delworth and Dixon 2006). But the competing roles of GHGs and AAs in forcing the twentieth-century Indian Ocean warming are not well known.

Here we examine the competing effects of GHGs and AAs in the Indian Ocean warming and their mechanisms during 1870–2005. The relative contributions of GHGs and AAs, via direct and indirect aerosol effects, to the Indian Ocean warming are evaluated individually. The mechanisms for the SST change patterns under different forcings are investigated by diagnosing the mixed layer heat budget. The roles of GHGs and AAs in the formation of positive Indian Ocean dipole (IOD)-like warming pattern are examined. We show evidence that the warming trend is caused by the increased GHGs, but the emission of AAs has slowed down the warming trend mainly via indirect aerosol effects. Here we show how GHGs and AAs have competed with each other in forming the Indian Ocean basinwide warming pattern as well as the IOD-like warming pattern along the equator.

The remainder of the paper is organized as follows. The models, data, and analysis methods are described in section 2. The results of the analysis are presented in section 3. In this section, the relative contributions of

GHGs and AAs to the Indian Ocean warming trend are assessed. Then we investigate the mechanism for the basinwide warming pattern by the diagnosis of the Indian Ocean mixed layer heat budget. Finally, the contributions of GHGs and AAs to the formation of IOD-like warming pattern are further elucidated. A discussion is given in section 4 along with a summary.

2. Model, data, and analysis methods

a. Model and experiments

We use 17 CGCMs contributing to phase 5 of the Coupled Model Intercomparison Project (CMIP5; http://pcmdi9.llnl.gov; Taylor et al. 2012). The models are listed in Table 1. All the models have been regridded to the horizontal resolution of 2.8° × 2.8°, which is the lowest resolution among these 17 CMIP5 models, and we convert the monthly products to yearly variables for analysis. The multimodel ensemble (MME) is defined as the arithmetic mean of models, with the same weight for each model. The GHG forcing is estimated from the MME of the 17 models. We estimate the total AA effect from the MME of 13 models, which include both the direct and indirect effects of aerosols. The direct effect of AAs is estimated from the MME of four models, which consider direct effect alone (Table 1). Four sets of numerical simulations are used in this study (http://pcmdi9.llnl.gov/esgf-web-fe/live). The details are described below.

1) The twentieth-century historical climate simulations (all forcing runs). The forcing data are from the CMIP5 for the Fifth Assessment Report (AR5) of the Intergovernmental Panel on Climate Change (IPCC). The scenario data include natural agent changes (mainly solar and volcanic) and anthropogenic agent changes (e.g., well-mixed greenhouse gases, aerosols, ozone, and land-use changes) (Taylor et al. 2012).
2) GHG-only forcing simulations (historicalGHG runs). The simulations are forced under well-mixed GHGs as in the all forcing run, but other agents are fixed at the preindustrial level.
3) Natural-only forcing simulations (historicalNat runs). The natural agents are the same as those used in the all forcing run, but the anthropogenic agents are fixed at the preindustrial level.
4) AA-only forcing simulations (historicalMisc runs). Note that the level of complexity and the range of aerosol species differ among different models.

We choose the common period across 1870–2005 in different models for our analysis. The specific forcing agents of GHGs and aerosols in each CMIP5 model are listed in Table 2.

b. Data description

The observed dataset used in this study is the monthly observed SST data from the Hadley Centre Global Sea Ice and Sea Surface Temperature dataset (HadISST) (Rayner et al. 2003) from 1870 to 2005.

c. Analysis methods

Following Taylor et al. (2012), the contributions of AAs can be estimated by using all forcing runs minus GHG-only forcing runs and natural-only forcing runs (Meehl et al. 2004; Taylor et al. 2012). To verify this hypothesis in CMIP5 models, we choose 10 CMIP5 models that have AA-only forcing simulations, named "historicalMisc runs" for comparison (Table 1). By comparison between the two results of AA effects, we find that most models show similar SST trends in the Indian Ocean in the two methods, but differences are also evident in FGOALS-g2 and CCSM4 (Fig. 1; note that expansions of CMIP5 model acronyms are given in Table 1). The possible factors inducing these differences are discussed in section 4a.

The changes of SST can be diagnosed by a mixed layer heat budget analysis. The SST tendency equation is written as

$$C\frac{\partial T'}{\partial t} = D'_o + Q'_{\text{net}}, \tag{1}$$

where T' is SST change (here we assume that SST equals mixed-layer mean temperature), C is the heat capacity of the mixed layer, Q'_{net} represents the change in the net surface heat flux into the ocean (positive downward), and D'_o denotes the ocean heat transport effect due to three-dimensional advection and mixing. At the interdecadal and longer time scales, the SST tendency goes to zero (Xie et al. 2010; Schneider and Fan 2012) and thus Eq. (1) can be reduced to

$$D'_o = -Q'_{\text{net}}. \tag{2}$$

Based on Eq. (2), we can infer the oceanic processes effect from the net surface heat flux.

To obtain the SST changes, the surface latent heat flux (Q'_E) is regarded as a mixture of ocean response (Q'^{o}_E) and atmospheric forcing (Q'^{a}_E) (de Szoeke et al. 2007; Xie et al. 2010; Du and Xie 2008). The former represents the Newtonian cooling effect, and the latter part is calculated as a residual. As a result, the surface latent heat flux from atmosphere is calculated as

$$Q'^{a}_E = Q'_E - \alpha\overline{Q_E}T'. \tag{3}$$

Then the effects of atmospheric processes (Q'_a) can be obtained as follows:

TABLE 1. Model names and institutions used in this study. The number 1 (0) denotes the corresponding experiment is (is not) used in our study, or the indirect aerosol effect is (is not) considered in the model. Note that the historicalMisc (AA) simulations of GISS-E2-R and GISS-E2-H used here are based on concentrations, not those on emissions.

No.	Modeling center	CMIP5 model name	Historical	HistoricalGHG	HistoricalNat	Historical Misc(AA)	Indirect
1	MIROC	Model for Interdisciplinary Research on Climate, Earth System Model (MIROC-ESM)	1	1	1	0	1
2	Meteorological Research Institute (MRI)	MRI Coupled Atmosphere–Ocean General Circulation Model, version 3 (MRI-CGCM3)	1	1	1	0	1
3	Centre National de Recherches Météorologiques (CNRM)– Centre Européen de Recherche et de Formation Avancée en Calcul Scientifique (CERFACS)	CNRM Coupled Global Climate Model, version 5 (CNRM-CM5)	1	1	1	0	1
4	Commonwealth Scientific and Industrial Research Organisation (CSIRO)–Queensland Climate Change Centre of Excellence QCCCE	CSIRO Mark, version 3.6.0 (CSIRO-Mk3.6.0)	1	1	1	1	1
5	National Center for Atmospheric Research (NCAR)	Community Climate System Model, version 4 (CCSM4)	1	1	1	1	0
6	National Oceanic and Atmospheric Administration (NOAA)/Geophysical Fluid Dynamics Laboratory (GFDL)	GFDL Climate Model, version 3 (GFDL-CM3)	1	1	1	1	1
7	L'Institut Pierre-Simon Laplace (IPSL)	IPSL Coupled Model, version 5, coupled with Nucleus for European Modelling of the Ocean (NEMO), low resolution (IPSL-CM5A-LR)	1	1	1	1	1
8	National Aeronautics and Space Administration (NASA) Goddard Institute for Space Studies (GISS)	GISS Model E2, coupled with the Russell ocean model (GISS-E2-R)	1	1	1	1	1
9	State Key Laboratory of Numerical Modeling for Atmospheric Sciences and Geophysical Fluid Dynamics (LASG)–Center for Earth System Science (CESS)	Flexible Global Ocean–Atmosphere–Land System Model gridpoint, version 2 (FGOALS-g2)	1	1	1	1	1
10	Beijing Climate Center (BCC)	BCC, Climate System Model, version 1.1 (BCC_CSM1.1)	1	1	1	0	0
11	Beijing Normal University (BNU)	BNU Earth System Model (BNU-ESM)	1	1	1	0	0
12	NOAA/GFDL	GFDL Earth System Model with Modular Ocean Model 4 (MOM4) component (GFDL-ESM2M)	1	1	1	1	0
13	Canadian Centre for Climate Modelling and Analysis (CCCma)	Second Generation Canadian Earth System Model (CanESM2)	1	1	1	1	1
14	Met Office Hadley Centre (MOHC)	Hadley Centre Global Environment Model, version 2–Earth System (HadGEM2-ES)	1	1	1	0	1
15	Norwegian Climate Centre (NCC)	Norwegian Earth System Model, version 1 (intermediate resolution) (NorESM1-M)	1	1	1	1	1
16	MIROC	MIROC Earth System Model, chemistry coupled (MIROC-ESM-CHEM)	1	1	1	0	1
17	NASA GISS	GISS Model E2, coupled with the Hybrid Coordinate Ocean Model (HYCOM) (GISS-E2-H)	1	1	1	1	1

TABLE 2. The forcing agents in the CMIP5 models global climate projections. Entries are as follow: BC: black carbon; OC: organic carbon; CAE: cloud albedo effect; CLE: cloud lifetime effect; Ds: dust; Vl: volcanic; SS: sea salt; LU: land use; Sl: solar.

Model	GHGs	Aerosols	Other
MIROC-ESM	CO_2, CH_4, N_2O, CFCs	SO_4, BC, OC, CAE, CLE, Ds, Vl, SS	Trop O_3, Strat O_3, LU, Sl
MRI-CGCM3	CO_2, CH_4, N_2O, CFCs	SO_4, BC, OC, CAE, CLE, Ds, Vl, SS	Trop O_3, Strat O_3, LU, Sl
CNRM-CM5	CO_2, CH_4, N_2O, CFCs	SO_4, BC, OC, CAE, Ds, Vl, SS	Trop O_3, Strat O_3, Sl
CSIRO-Mk3.6.0	CO_2, CH_4, N_2O, CFCs	SO_4, BC, OC, CAE, Ds, Vl, SS	Trop O_3, Strat O_3, Sl
CCSM4	CO_2, CH_4, N_2O, CFCs	SO_4, BC, OC, Ds, Vl, SS	Trop O_3, Strat O_3, LU, Sl
GFDL-CM3	CO_2, CH_4, N_2O, CFCs	SO_4, BC, OC, CAE, CLE, Ds, Vl, SS	Trop O_3, Strat O_3, LU, Sl
IPSL-CM5A-LR	CO_2, CH_4, N_2O, CFCs	SO_4, BC, OC, CAE, Ds, Vl, SS	Trop O_3, Strat O_3, LU, Sl
GISS-E2-R	CO_2, CH_4, N_2O, CFCs	SO_4, BC, OC, CAE, Ds, Vl, SS, Nitrate	Trop O_3, Strat O_3, LU, Sl
FGOALS-g2	CO_2, CH_4, N_2O, CFCs	SO_4, BC, OC, CAE, CLE, Ds, Vl, SS	Trop O_3, Strat O_3, Sl
BCC_CSM1.1	CO_2, CH_4, N_2O, CFCs	SO_4, BC, OC, Ds, Vl, SS	Trop O_3, Strat O_3, Sl
BNU-ESM	CO_2, CH_4, N_2O, CFCs	SO_4, BC, OC, Ds, Vl, SS	Trop O_3, Strat O_3, Sl
GFDL-ESM2M	CO_2, CH_4, N_2O, CFCs	SO_4, BC, OC, Ds, Vl, SS	Trop O_3, Strat O_3, LU, Sl
CanESM2	CO_2, CH_4, N_2O, CFCs	SO_4, BC, OC, CAE, Ds, Vl, SS	Trop O_3, Strat O_3, LU, Sl
HadGEM2-ES	CO_2, CH_4, N_2O, CFCs	SO_4, BC, OC, CAE, CLE, Ds, Vl, SS	Trop O_3, Strat O_3, LU, Sl
NorESM1-M	CO_2, CH_4, N_2O, CFCs	SO_4, BC, OC, CAE, CLE, Ds, Vl, SS	Trop O_3, Strat O_3, LU, Sl
MIROC-ESM-CHEM	CO_2, CH_4, N_2O, CFCs	SO_4, BC, OC, CAE, CLE, Ds, Vl, SS	Trop O_3, Strat O_3, LU, Sl
GISS-E2-H	CO_2, CH_4, N_2O, CFCs	SO_4, BC, OC, CAE, Ds, Vl, SS, Nitrate	Trop O_3, Strat O_3, LU, Sl

$$Q'_a = Q'_S + Q'_L + Q'_H + Q^{a'}_E, \tag{4}$$

where Q'_S is surface shortwave radiation changes, Q'_L is surface longwave radiation changes, and Q'_H is surface sensible heat flux changes. Finally, the patterns of SST trend (T') are by definition determined by the trends in atmospheric forcing via radiative and turbulent fluxes (Q'_a) and the change in heat supplied by ocean heat transport (D'_o) (Xie et al. 2010). The climatological latent heat flux ($\overline{Q_E}$) influences the amplitude of SST changes, written as

$$T' = \frac{(D'_o + Q'_a)}{\alpha \overline{Q_E}}. \tag{5}$$

The coefficient α is $LR_v^{-1}T^{-2}$ based on the Clausius–Clapeyron equation. In the present study, α is about $0.06\,\mathrm{K}^{-1}$. For more details of the calculation methods, readers can refer to Xie et al. (2010) and Dong et al. (2014). In this study, we first apply the heat budget analysis for each CMIP5 model. Then atmosphere processes and ocean processes are discussed based on the result of MME.

The linear trends are tested by Student's t test (Wilks 1995). We do not remove the climate drift when calculating the trends of different forcing experiments for the following reasons: the role of climate drift is smaller in CMIP5 models (Jones et al. 2013); it will be reduced in MME due to the asymmetric direction of drift across different models (Sen Gupta et al. 2012); and the trend of the preindustrial control run may be long-term internal variability that may or may not happen in a parallel experiment when additional forcing has been applied (Jones et al. 2013).

3. Results

a. *The relative contributions of GHGs and AAs to the Indian Ocean warming*

Time evolutions from observations and different forcing simulations of the MME are compared in Fig. 2. A significant warming trend during 1870–2005 is seen in the observations, especially during the last half of the twentieth century (Fig. 2a). The warming trend is well reproduced by all forcing runs (Fig. 2b). GHGs forcing dominates the warming trend in the Indian Ocean, and the warming effect is evident throughout the twentieth century (Fig. 2c). The total AA effect (including both direct and indirect effects) cools the basin-averaged SST and slows down the warming trend (Fig. 2d). Note that after the 1950s, the cooling is rapid due to the large

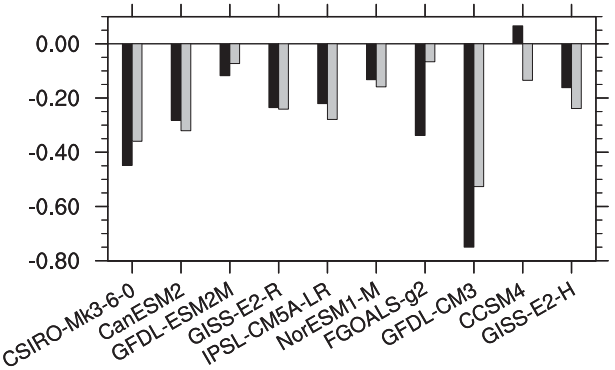

FIG. 1. Two methods for evaluating AA forcing: all forcing runs minus natural-only forcing runs and GHG-only forcing runs (all-GHG-Nat) (black bars), and AA-only forcing (historicalMisc) runs (gray bars) from 10 CMIP5 models. Units: K $(100\,\mathrm{yr})^{-1}$.

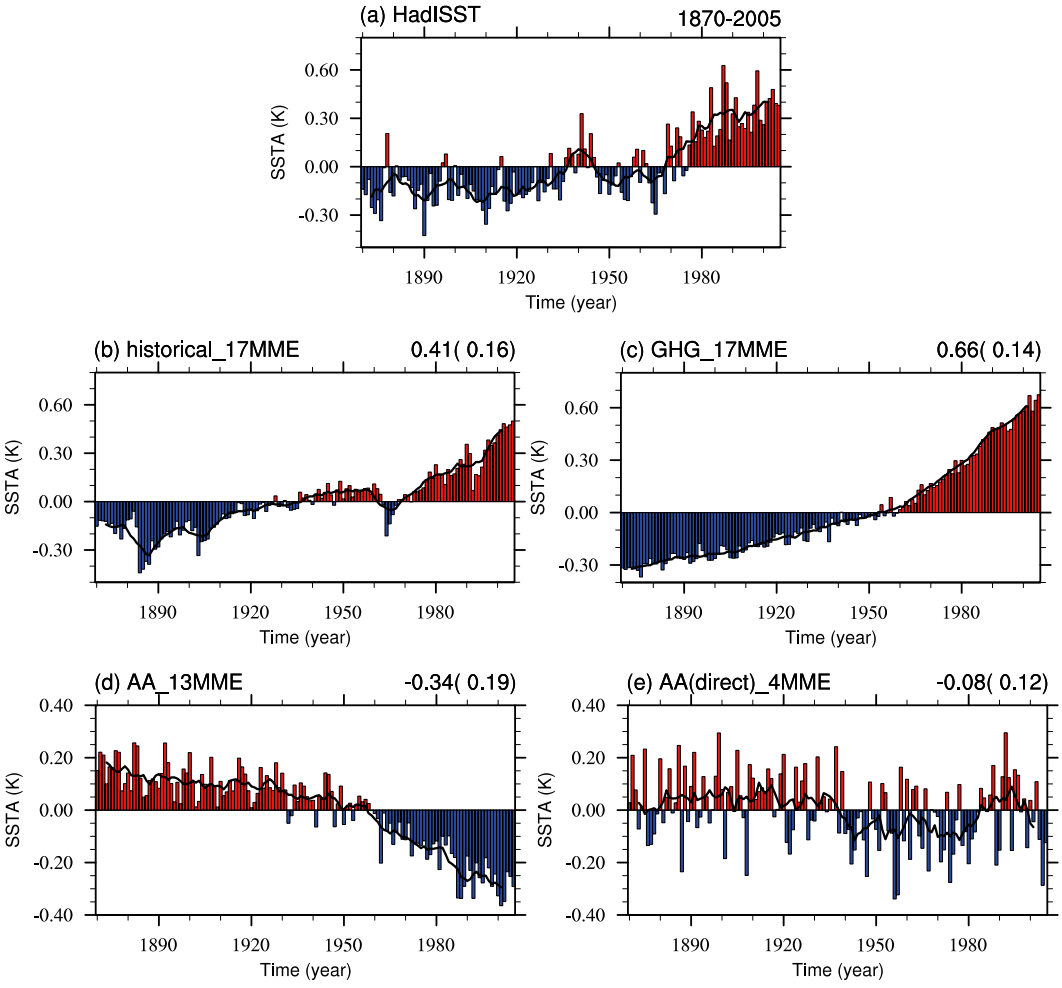

FIG. 2. Time series of Indian Ocean (40°S–15°N, 40°–100°E) annual mean (bar) and 8-yr running average (line) sea surface temperature anomaly (SSTA) from (a) observations, (b) all forcing runs of 17 models from the MME, (c) GHG-only forcing runs of 17 models of the MME, (d) AA-only forcing of 13 models from the MME that include both direct and indirect effects, and (e) AA-only forcing of four models from the MME that only include direct effects. SSTA is relative to the period of 1870–2005 mean. Units: K. The numbers on the top right of (b)–(e) denote the trend values and standard deviation of intermodel variations, respectively.

emission of AAs with postwar economic growth (Xie et al. 2013). However, the cooling effect is weakened when only the direct effect of AAs is considered (Fig. 2e). The conclusion will not change when we add or subsample the ensemble member of each model (not shown).

Comparing the warming trends during 1870–2005 between the observation and simulations, the observed trend of 0.40 K century^{-1} is well captured by all forcing run of 0.41 $\pm$ 0.16 K century^{-1} (standard deviation of intermodel variations). Under GHG-only forcing, the warming trend is 0.66 $\pm$ 0.14 K century^{-1}, which is stronger than both the observations and the all forcing run. Among all the 17 CMIP5 models, the trends under GHG forcing are positive, with contributions to the all forcing run ranging from 87.1% in CCSM4 to 520% in GFDL-CM3, with the MME accounting for about 163.6% (Fig. 3). However, the emission of AAs has slowed down the warming trend. The results show that AAs have negative contributions to the warming, except for CCSM4 (Fig. 3). Based on the result of the MME, AAs account for about −72.7% of the all forcing run trend. If only the direct effect of AAs is considered, there is a weak cooling trend of -0.08 ± 0.12 K century^{-1} (Fig. 2e). But if both direct and indirect effects are included, the cooling trend is enhanced to -0.34 ± 0.19 K century^{-1} (Fig. 2d), offsetting roughly half of GHGs warming. As the trends in all forcing run, GHG-only forcing run, and AA-only run are 0.41, 0.66, and −0.34 respectively, the extra warming may be due to their different model numbers for the ensemble or coming from the natural-only forcing runs

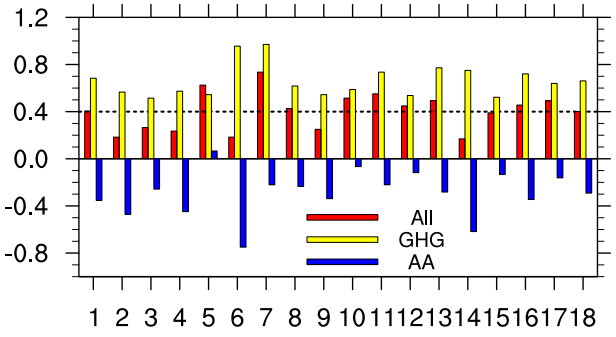

FIG. 3. The SST trends during 1870–2005 averaged in Indian Ocean (40°S–15°N, 40°–100°E) under all forcing runs, GHG-only forcing runs, and AA-only forcing (historical–historicalGHG–historicalNat) from 17 CMIP5 models as shown in Table 1 and the MME of them (number 18). The dashed line represents the trends in observation. Units: K $(100\,\mathrm{yr})^{-1}$.

or the nonlinear interactions among different forcing. Therefore, the GHGs and AAs have imposed competing effects on the Indian Ocean SST changes. The AAs have slowed down the warming trend induced by increased GHGs.

The trend patterns of SST in the Indian Ocean during 1870–2005 from observations and different forcing simulations of MME are shown in Fig. 4. The observations show a warming trend in the whole Indian Ocean basin (the basinwide warming pattern), with the maximum in the equatorial western Indian Ocean (the positive IOD-like warming pattern) (Du and Xie 2008; Zheng et al. 2010; Xie et al. 2010; Cai et al. 2013; see Fig. 4a), which is captured by the MME of all forcing run (Fig. 4b). Under GHG-only (AA-only) forcing, the Indian Ocean shows a basinwide warming (cooling) pattern (Figs. 4c,d). The magnitude of warming under GHG forcing (Fig. 4c) is stronger than that in the observations (Fig. 4a) and all forcing run (Fig. 4b). The warming (cooling) rate response to GHG (AA) forcing in the northern basin is larger than that in the southern basin (Figs. 4c,d). In contrast, if only the AA direct effect is considered, the SST trend shows a weak cooling trend in the northwestern basin and southwestern basin and a negative IOD-like pattern along the equator (Fig. 4e).

Note that the time series and warming pattern of the Indian Ocean derived from the extended reconstructed SST (ERSST3) data (Smith et al. 2008) show similar results to HadISST (not shown). The most significant characteristics of the Indian Ocean warming pattern (i.e., the basinwide warming pattern and the equatorial positive IOD-like warming pattern; Fig. 4a) are well reproduced by the all forcing run from the ensemble of 17 CMIP5 models (Fig. 4b). Thus we further address the mechanism for the warming pattern formation and the roles of GHGs and AAs based on this ensemble in the following section.

b. *Mechanisms for the Indian Ocean basinwide warming pattern*

The mechanism for the formation of the basinwide warming pattern is investigated through a mixed layer heat budget analysis introduced in section 2c. The basinwide warming evident in the GHG-forced pattern is dominated by the atmospheric heat flux term (Q'_a, Fig. 5a). In contrast, the ocean processes (D'_o) have a smaller contribution to the basinwide SST trend (Fig. 5d). This result is different from that of Alory and Meyers (2009), even when we change our analyzed period to 1960–99 to match theirs (not shown). Alory and Meyers (2009) suggest that the SST warming in the equatorial Indian is mostly due to oceanic processes. The reason may be the different considerations of the Newtonian cooling effect in these two heat budget methods. In addition, the method in Alory and Meyers (2009) mainly concentrates on a regional average and regards it as a box, whereas Xie et al. (2010) show the patterns of each process. On the other hand, the method of Xie et al. (2010) can only be applied to interdecadal or longer time scales.

The atmospheric forcing via radiative and turbulent fluxes (Q_a) can be further decomposed into four parts: surface shortwave radiation (Q_S), surface longwave radiation (Q_L), sensible heat flux (Q_H), and latent heat flux from the atmosphere (Q_E^a). Because of the small contribution of Q'_H, we only present the effects of Q'_S, Q'_L, and $Q_E^{a'}$. The positive contributions of Q'_L (Fig. 5j) and $Q_E^{a'}$ (Fig. 5m) due to the increased GHGs are the most important in forming the basinwide warming trend. Under AA-only forcing, Q'_a cools the whole Indian Ocean (Fig. 5b). The reduction of Q'_S, Q'_L, and $Q_E^{a'}$ associated with the AA effect contributes to the basinwide cooling (Figs. 5h,k,n), competing with the warming effect of GHG forcing. As $Q_E^{a'}$ is largely determined by the changes of wind speed, we further analyze the trends of surface wind vector and surface wind speed under different forcing in Fig. 6. The trends of surface wind speed have similar distributions with the trends of $Q_E^{a'}$. Where the surface wind speed increases (decreases), the positive contribution of $Q_E^{a'}$ under GHG-only forcing is suppressed (enhanced) and negative contribution of $Q_E^{a'}$ under AA-only forcing is enhanced (suppressed) (Fig. 6). We find that there is an easterly wind anomaly along the equator under GHG forcing (Fig. 6a). Under AA forcing, the surface wind vector has no robust trend along the equator (Fig. 6b). However, a strong westerly wind anomaly occurs when only the direct AA effect is considered (Fig. 6c).

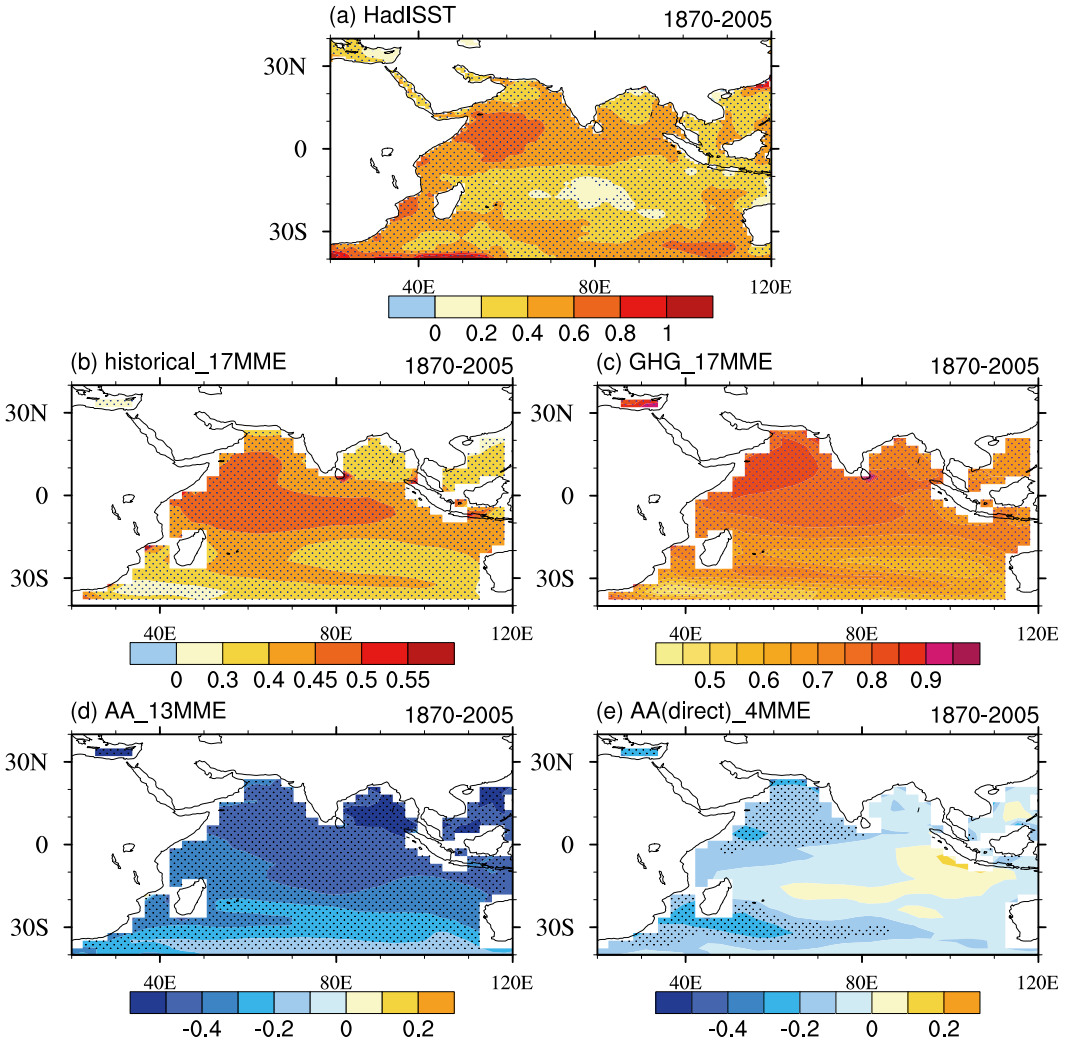

FIG. 4. The trends of SST in the Indian Ocean during 1870–2005 from (a) observations, (b) all forcing runs of a 17-model MME, (c) GHG-only forcing runs of a 17-model MME, (d) AA-only forcing of a 13-model MME, and (e) direct effects of AA-only forcing of a 4-model MME. The dotted areas are statistically significant at the 1% level by Student's t test. Note that the color scale intervals are not the same for each figure. Units: K $(100\,\mathrm{yr})^{-1}$.

The competing roles of GHGs and AAs in Q'_L and Q'^{a}_{E} (Figs. 7a,b) and the cooling effect of AAs in Q'_S (Fig. 7c) are confirmed in most CMIP5 models. By comparing the atmospheric and oceanic processes between total AA effect (Figs. 5b,e,h,k,n) and direct AA effect alone (Figs. 5c,f,i,l,o), we suggest that the cooling effect of AAs is primarily caused by indirect aerosol effect through atmospheric processes. The indirect effects of sulfate aerosols make clouds brighter (first indirect effect) or longer lasting (second indirect effect) (e.g., Ramaswamy et al. 2001; Lohmann and Feichter 2005), thereby altering the ocean surface heat fluxes. This result demonstrates that the aerosol–cloud interaction is important in the Indian Ocean SST change, and also reveals an improvement from CMIP3 (largely neglecting the aerosol–cloud interaction) to CMIP5 models. In addition, the basinwide SST trends under AAs forcing are linearly related to the trends of surface shortwave radiation, surface longwave radiation, and latent heat flux from the atmosphere, with surface longwave radiation and latent heat flux from the atmosphere of higher explained variance (Fig. 8). However, the linear relationship between SST trends and surface shortwave radiation trends is not significant given the nonuniform distribution of cloud, which can influence surface shortwave radiation to a great extent (Fig. 8a). Thus the larger negative trends of these three surface heat fluxes tend to cool the Indian Ocean under AA-only forcing.

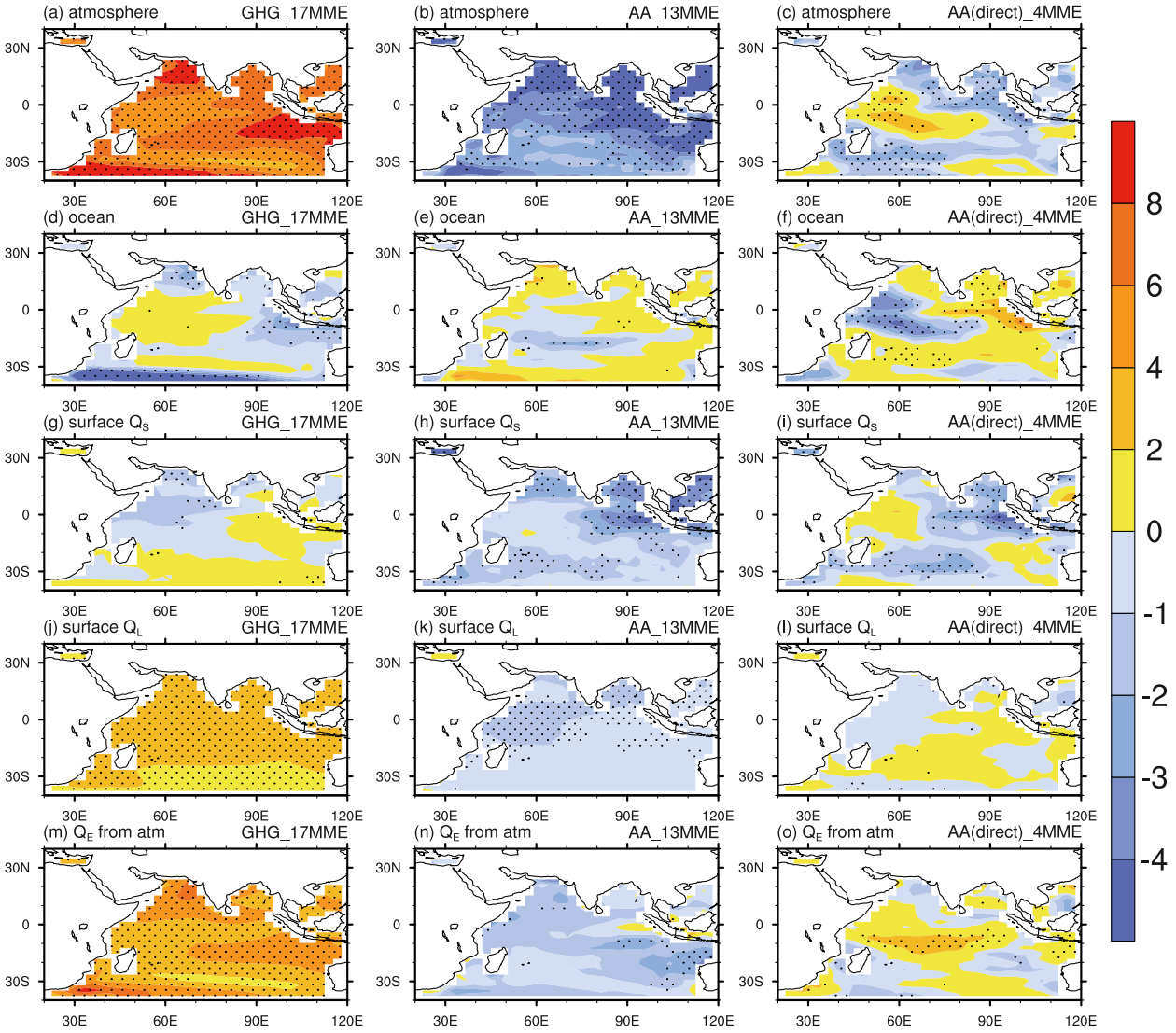

FIG. 5. The contributions of (a)–(c) atmospheric forcing (Q'_a), (d)–(f) ocean heat transport effect (D'_o), (g)–(i) surface shortwave radiation (Q'_S), (j)–(l) surface longwave radiation (Q'_L), and (m)–(o) latent heat flux from the atmosphere (Q'_E) for the (left) GHG-only forcing MME and (middle) AA-only forcing MME, and (right) the direct effect of AAs alone. An MME result is considered robust when more than 80% of the models have the same sign as the MME (shown as dotted in figures). Note that the color scale intervals are not the same for positive and negative values. Units: W m^{-2} (100 yr)$^{-1}$.

c. *Contributions of GHGs and AAs to the equatorial IOD-like warming pattern*

Previous studies indicated that the positive IOD-like warming pattern along the equator is mainly due to the slowdown of the Walker circulation under global warming, with an easterly wind anomaly and a shoaling thermocline and reduced SST warming in the eastern Indian Ocean (Vecchi and Soden 2007; Du and Xie 2008; Stowasser et al. 2009; Zheng et al. 2010; Xie et al. 2010; Dong et al. 2014). The scatterplots of the trends of east–west SST gradient versus the trends of surface zonal wind (the x-coordinate component of wind vector, commonly denoted as u) along the equator from all forcing runs of 17 CMIP5 models, as well as the MME, are presented (Fig. 9a). The trends of the east–west SST gradient have a good linear relationship with the trends of surface zonal wind along the equator, which is statistically significant at the 1% level. When there is an easterly wind anomaly along the equator, there tends to be a positive IOD-like warming pattern, and vice versa. The linear relationship also holds in the GHG-only forcing and AA-only forcing runs (not shown). Most models show easterly wind anomalies over 1870–2005 (negative zonal wind trend)

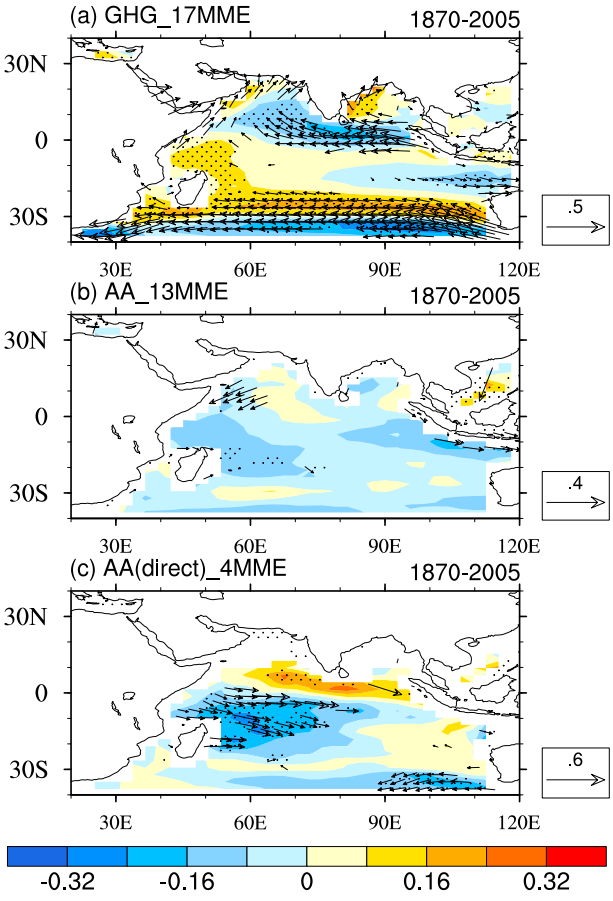

FIG. 6. The trends of surface wind vector and surface wind speed (shaded) in the Indian Ocean during 1870–2005 from (a) GHG-only forcing runs of a 17-model MME and (b) AA-only forcing runs of a 13-model MME, and (c) the direct effects of AAs of a 4-model MME. The wind trend is considered robust when more than 80% of the models have the same sign as the MME, as drawn (for wind vectors) and dotted (for wind speed) in figures. Units: $m\,s^{-1}\,(100\,yr)^{-1}$.

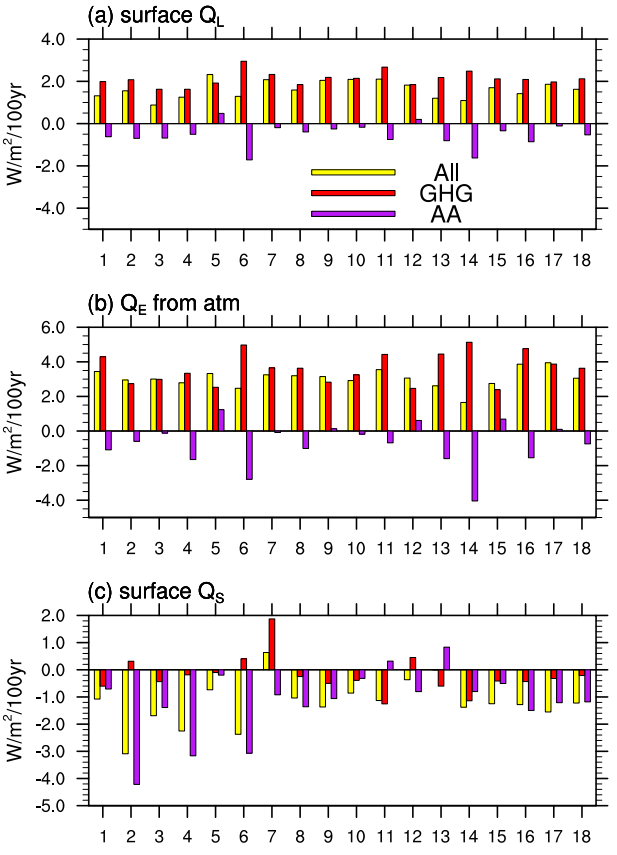

FIG. 7. The Indian Ocean averaged trends of (a) surface longwave radiation (Q'_L), (b) latent heat flux from atmosphere (Q'^{a}_{E}), and (c) surface shortwave radiation (Q'_S) under all forcing runs (yellow bars), GHG-only forcing runs (red bars), and AA-only forcing (purple bars) of 17 CMIP5 models as shown in Table 1 and the MME of them (number 18). Units: $W\,m^{-2}\,(100\,yr)^{-1}$.

along the equator and positive IOD-like warming patterns (positive trend of the east–west SST gradient) under all forcing runs (Fig. 9a). Thus the easterly wind anomaly along the equator is associated with the positive IOD-like warming pattern, which is consistent with some previous studies (e.g., Cai and Cowan 2013; Zheng et al. 2013).

To understand the relative roles of GHGs and AAs in the formation of the positive IOD-like warming pattern, we evaluate the trend of surface zonal wind along the Indian Ocean equator under different forcings (Fig. 9b). Based on the results of the MME, the surface easterly wind anomaly along the Indian Ocean equator of the all forcing run (orange bar) is attributed to anthropogenic forcing (red bar). The natural forcing results in a weaker westerly wind anomaly (yellow bar). The anthropogenic forcing is further divided into two parts: GHGs and aerosols. GHG forcing induces the easterly wind anomaly and accounts for a forcing equivalent to about 140.0% of the anthropogenic forcing (green bar), while the AAs forcing has a smaller contribution (purple bar). However, the direct effect of AAs alone induces surface westerly wind anomaly, which weakens the easterly wind anomaly from GHGs forcing (blue bar). This result complements the spatial pattern shown in Fig. 6. Such anomalous westerly wind is associated with the negative IOD-like SST pattern under the direct effect of AAs (Fig. 4e), and they are both amplified by Bjerknes feedback (Bjerknes 1969). Based on Bjerknes feedback, the negative IOD-like SST pattern under direct AA forcing induces the westerly wind anomalies, which uplift the thermocline and further cool the SST in the western basin, and contribute to SST warming via deeper thermocline in the eastern basin. It seems that the indirect AA effects act to mitigate the impact of the direct AA effects. Nevertheless, since there are only four models with a direct effect

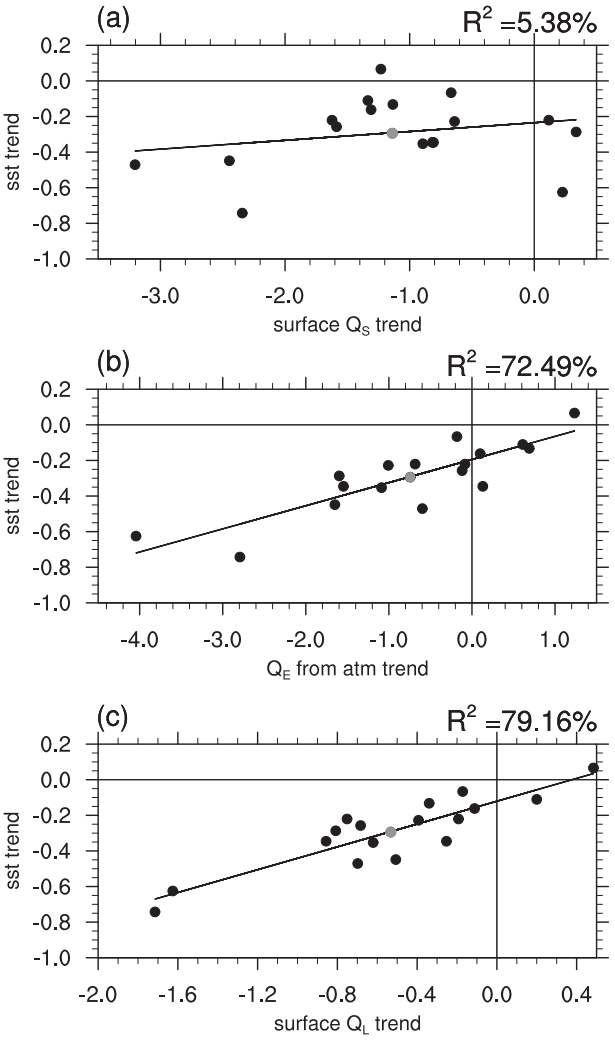

FIG. 8. The scatterplots of Indian Ocean averaged SST trends vs the trends of (a) surface shortwave radiation, (b) latent heat flux from atmosphere, and (c) surface longwave radiation under AA-only forcing from 17 CMIP5 models. Each black dot represents a CMIP5 model, and the gray dot represents the MME. The number on the top right denotes the squares of correlation coefficient.

of AAs alone forcing in our study, more models and simulations are needed for further confirmation.

Among the 17 CMIP5 models, 16 models exhibit an easterly wind anomaly due to the slowdown of the Walker circulation under GHG forcing (Fig. 9c). In contrast, the results under AA forcing show uncertainties among models. There are 11 models that show a westerly wind anomaly under AA forcing whereas six models show an easterly wind anomaly, but four do so with weak trends (Fig. 9d). Thus, we suggest that AA forcing, mainly via the direct aerosol effect, tends to result in a surface westerly wind anomaly and a negative IOD-like warming pattern along the equator, which offsets the effect of GHG forcing. In addition, by comparing the atmospheric and oceanic processes (Figs. 5a–f), we infer that GHG (direct AA) forcing dominates the formation of the positive (negative) IOD-like warming pattern, mainly via oceanic processes (Figs. 5d,f). The conclusion is consistent with that of our previous study (Dong et al. 2014), which reported that the oceanic process is the most important in forming the SST zonal dipole pattern in the Indian Ocean under the all forcing simulation.

4. Summary and discussion

a. Discussion

The method from Taylor et al. (2012) introduced in section 2c assumes that the effects of different forcing can cumulate linearly. Do the effects cumulate linearly or commingle with each other? We further choose two CMIP5 models that have NoAA (all forcing agents are same as historical, but no anthropogenic aerosols change) runs and Ant (anthropogenic-only forcing) runs for discussion. By comparison of the results between ALL-NoAA and AA-only forcing, we find that both models show similar trends in the two methods of estimating AA effects (Fig. 10a). In addition, the SST trends of the Indian Ocean under anthropogenic-only forcing estimated from ALL-Nat and Ant-only forcing are also similar (Fig. 10b). The results demonstrate that the linearity assumption can be applied to estimate the AA forcing effects in our study.

The limitations of the current study should be noted. There are evident differences in FGOALS-g2 and CCSM4 between the two methods in examining the AA forcing (Fig. 1). When we checked other CCSM4 runs for comparison, there still existed evident differences between the two methods (not shown). The difference may be related to the following aspects. 1) The effects of different forcing may have nonlinear parts. 2) The forcings in the two methods are not exactly the same. For example, FGOALS-g2 (CCSM4) includes ozone forcing (ozone forcing and land-use change forcing) in the historical–historicalGHG–historicalNat runs, but these forcing agents were not specified in the historicalMisc (AA) run. 3) The effect of each forcing may be model dependent.

The ozone forcing is included in all the 17 models (Table 2), and its depletion could lead to a similar impact to an increase in GHGs on atmospheric circulation (Sigmond et al. 2011). However, the warming trend under ozone forcing is not stronger based on CMIP3 models (Alory et al. 2007). As ozone forcing is included in the historical–historicalGHG–historicalNat runs but not in historicalMisc, we further clarify the individual effect of

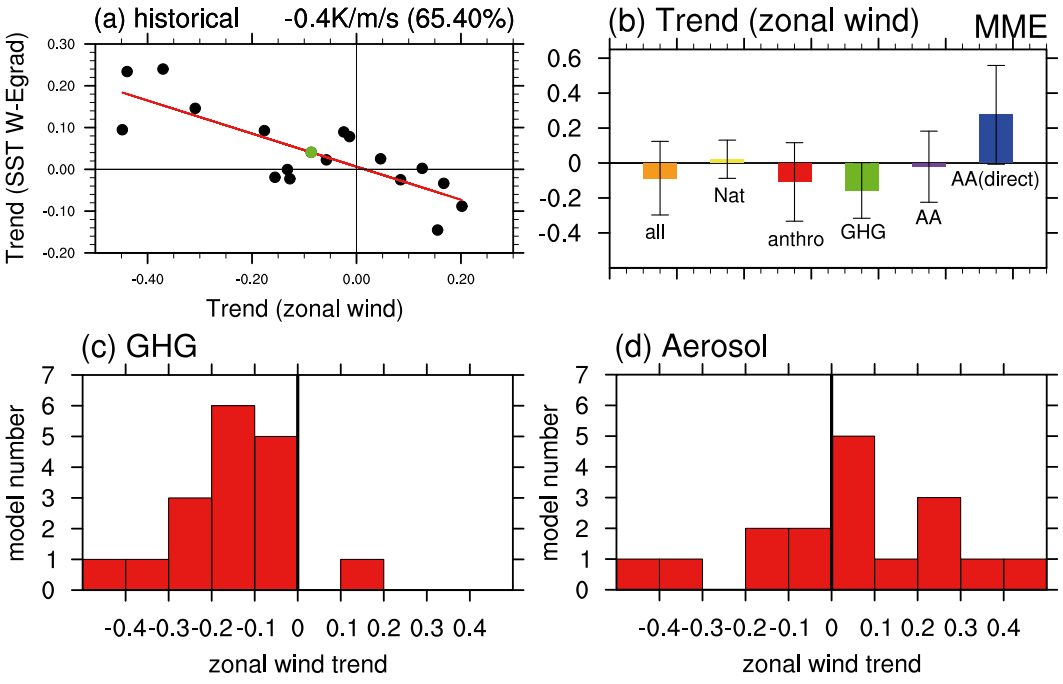

FIG. 9. (a) The scatterplots of the trends of east–west SST gradient (y axis) vs the trends of surface zonal wind (the x-coordinate component of wind vector, commonly denoted as u) along the equator (x axis) from all forcing runs of 17 CMIP5 models. The east–west SST gradient is defined as the SST difference between the western basin (5°S–5°N, 50°–65°E) and eastern basin (5°S–5°N, 85°–100°E). The surface zonal wind along the equator is the average of 5°S–5°N, 50°–90°E. The numbers on the top right denotes the regression coefficient and the squares of correlation coefficient of the scatters. Each black dot represents a CMIP5 model, and the green dot represents MME. (b) The trends of zonal wind along the Indian Ocean equator from MME under all forcing, natural forcing, anthropogenic forcing, GHG forcing, AA forcing include direct and indirect effects, and AA direct effects alone [units: $\mathrm{m\,s^{-1}}$ $(100\,\mathrm{yr})^{-1}$]. The anthropogenic forcing is estimated by the all forcing run minus the natural forcing run. The error bars show the trend values plus/minus the standard deviation of intermodel variations. The histogram of the surface zonal wind along the equator in the Indian Ocean is based on the 17 CMIP5 model integrations under (c) GHG forcing and (d) AA forcing.

ozone and AAs by using four models with an ozone-only forcing run (Fig. 10c). The results show that ozone depletion induces a warming trend in the Indian Ocean in all four models, but with weaker strength compared to that under GHG-only forcing. The warming effect of ozone depletion may weaken the cooling effect of AAs in the historical–historicalGHG–historicalNat method.

Because of the close proximity of India and the Arabian deserts, the role of mineral dust and black carbon in changing the Indian Ocean SST should be taken into consideration. Numerical experiments show that the heating of the atmosphere by dust transported from Arabian deserts and black carbon from local emissions can lead to a local lower tropospheric warming over these regions and surface warming over the Tibetan Plateau (Lau et al. 2010). As there are not black carbon–only forcing runs in CMIP5 models, we can estimate its effect by conducting numerical experiments in future work as conducted by studies such as Ganguly et al. (2012).

b. *Summary*

The main motivation of the present study is to examine the competing effects of GHGs and AAs in the Indian Ocean warming and their mechanisms during 1870–2005. Four sets of experiments—twentieth-century historical runs, GHG-only forcing runs, natural-only forcing runs, and AA-only forcing runs—are used in this study. The relative contributions of GHGs and AAs, through direct and indirect aerosol effects, to the Indian Ocean warming are evaluated individually. The mechanisms for the basinwide warming pattern under different forcings are investigated by diagnosing the mixed layer heat budget. The roles of GHGs and AAs in forming the positive IOD-like warming pattern are examined. The main conclusions are listed below.

1) The emission of AAs has slowed down the warming trend of Indian Ocean in the twentieth century. The Indian Ocean warming trend during 1870–2005 ($0.40\,\mathrm{K\,century^{-1}}$) is mainly caused by GHG forcing

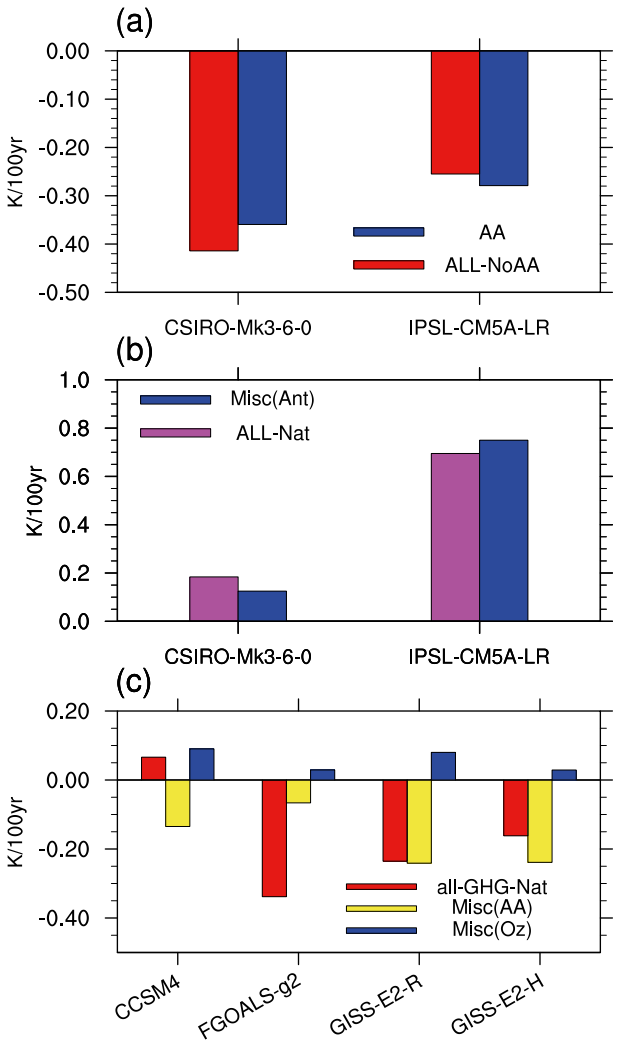

FIG. 10. The SST trends during 1870–2005 averaged in the Indian Ocean (40°S–15°N, 40°–100°E) for (a) AA-only forcing runs (historicalMisc) (blue bars) and all forcing runs minus NoAA runs (ALL-NoAA) (red bars) from two CMIP5 models. (b) Anthropogenic-only forcing runs (historicalMisc) (blue bars) and all forcing runs minus natural-only forcing runs (ALL-Nat) (purple bars) from two CMIP5 models. (c) All forcing runs minus natural-only forcing runs and GHG-only forcing runs (all-GHG-Nat; red bars) and AA-only forcing runs (historicalMisc; yellow bars) and ozone-only forcing runs (blue bars) from four CMIP5 models. Units: K $(100\,\mathrm{yr})^{-1}$.

$(0.66\,\mathrm{K\,century}^{-1})$. With AA forcing, mainly via the indirect aerosol effect, the warming trend has been slowed down by $0.34\,\mathrm{K\,century}^{-1}$. The cooling effect is weakened when only the direct effect of AAs is considered. Thus, the aerosol–cloud interaction is important in the Indian Ocean SST change.

2) GHGs and AAs play competing roles in forming both the Indian Ocean basinwide warming pattern and the positive IOD-like warming pattern along the equator [the two characteristics of the Indian Ocean warming pattern, but not the same as the Indian Ocean basin-wind mode (IOBM) and dipole mode (IODM) at the interannual scale]. For the basinwide pattern, both the warming effect of GHGs and cooling effect of AAs through the indirect effect are established through atmospheric processes. The positive contributions of surface latent heat flux from the atmosphere and surface longwave radiation due to GHG forcing dominate the basinwide warming, while the reductions of surface shortwave radiation, surface longwave radiation, and latent heat flux from the atmosphere associated with AAs induce the basinwide cooling.
3) The positive IOD-like warming pattern is seen in association with the surface easterly wind anomaly along the equator, which is mainly associated with anthropogenic forcing. GHG forcing dominates the easterly wind anomaly; however, this is weakened by the direct effect of AAs.

Acknowledgments. This work is supported by the National Natural Science Foundation of China under Grants 41125017 and 41330423, and the National Program on Key Basic Research Project (2012CB955202). We acknowledge the World Climate Research Programme's Working Group on Coupled Modeling, which is responsible for CMIP5, and we thank the climate modeling groups for producing and making available their model output.

REFERENCES

Alory, G., and G. Meyers, 2009: Warming of the upper equatorial Indian Ocean and changes in the heat budget (1960–99). *J. Climate,* **22,** 93–113, doi:10.1175/2008JCLI2330.1.

——, S. Wijffels, and G. Meyers, 2007: Observed temperature trends in the Indian Ocean over 1960–1999 and associated mechanisms. *Geophys. Res. Lett.,* **34,** L02606, doi:10.1029/2006GL028044.

Ashok, K., Z. Guan, and T. Yamagata, 2003: Influence of the Indian Ocean dipole on the Australian winter rainfall. *Geophys. Res. Lett.,* **30,** 1821, doi:10.1029/2003GL017926.

Barnett, T. P., D. W. Pierce, K. M. AchutaRao, P. J. Gleckler, B. D. Santer, J. M. Gregory, and W. M. Washington, 2005: Penetration of human-induced warming into the world's oceans. *Science,* **309,** 284–287, doi:10.1126/science.1112418.

Bjerknes, J., 1969: Atmospheric teleconnections from the equatorial Pacific. *Mon. Wea. Rev.,* **97,** 163–172, doi:10.1175/1520-0493(1969)097<0163:ATFTEP>2.3.CO;2.

Booth, B. B. B., N. J. Dunstone, P. R. Halloran, T. Andrews, and N. Bellouin, 2012: Aerosols implicated as a prime driver of twentieth-century North Atlantic climate variability. *Nature,* **484,** 228–232, doi:10.1038/nature10946.

Cai, W., and T. Cowan, 2013: Why is the amplitude of the Indian Ocean dipole overly large in CMIP3 and CMIP5 climate

models? *Geophys. Res. Lett.,* **40,** 1200–1205, doi:10.1002/grl.50208.

——, D. Bi, J. Church, T. Cowan, M. Dix, and L. Rotstayn, 2006: Panoceanic response to increasing anthropogenic aerosols: Impacts on the Southern Hemisphere oceanic circulation. *Geophys. Res. Lett.,* **33,** L21707, doi:10.1029/2006GL027513.

——, T. Cowan, M. Dix, L. Rotstayn, J. Ribbe, G. Shi, and S. Wijffels, 2007: Anthropogenic aerosol forcing and the structure of temperature trends in the southern Indian Ocean. *Geophys. Res. Lett.,* **34,** L14611, doi:10.1029/2007GL030380.

——, ——, S. Godfrey, and S. Wijffels, 2010: Simulations of processes associated with the fast warming rate of the southern midlatitude ocean. *J. Climate,* **23,** 197–206, doi:10.1175/2009JCLI3081.1.

——, X. Zheng, E. Weller, M. Collins, T. Cowan, M. Lengaigne, W. Yu, and T. Yamagata, 2013: Projected response of the Indian Ocean dipole to greenhouse warming. *Nat. Geosci.,* **6,** 999–1007, doi:10.1038/ngeo2009.

Chang, C.-P., and T. Li, 2000: A theory of the tropical tropospheric biennial oscillation. *J. Atmos. Sci.,* **57,** 2209–2224, doi:10.1175/1520-0469(2000)057<2209:ATFTTT>2.0.CO;2.

Chang, C.-Y., J. C. H. Chiang, M. F. Wehner, A. R. Friedman, and R. Ruedy, 2011: Sulfate aerosol control of tropical Atlantic climate over the twentieth century. *J. Climate,* **24,** 2540–2555, doi:10.1175/2010JCLI4065.1.

Chen, W.-T., A. Nenes, H. Liao, P. J. Adams, J.-L. F. Li, and J. H. Seinfeld, 2010: Global climate response to anthropogenic aerosol indirect effects: Present day and year 2100. *J. Geophys. Res.,* **115,** D12207, doi:10.1029/2008JD011619.

Chiang, J. C. H., C.-Y. Chang, and M. F. Wehner, 2013: Long-term behavior of the Atlantic interhemispheric SST gradient in the CMIP5 historical simulations. *J. Climate,* 26, 8628–8640, doi:10.1175/JCLI-D-12-00487.1.

Chu, C., X.-Q. Yang, X. Ren, and T. Zhou, 2013: Response of Northern Hemisphere storm tracks to Indian–western Pacific Ocean warming in atmospheric general circulation models. *Climate Dyn.,* **40,** 1057–1070, doi:10.1007/s00382-013-1687-y.

Collier, M., L. D. Rotstayn, K. Y. Kim, A. C. Hirst, and S. J. Jeffrey, 2013: Ocean circulation response to anthropogenic aerosol and greenhouse gas forcing in the CSIRO-Mk3.6 climate model. *Aust. Meteor. Oceanogr. J.*, **63,** 27–39.

Cowan, T., and W. Cai, 2013: The response of the large-scale ocean circulation to 20th century Asian and non-Asian aerosols. *Geophys. Res. Lett.,* **40,** 2761–2767, doi:10.1002/grl.50587.

——, ——, A. Purich, L. Rotstayn, and M. H. England, 2013: Forcing of anthropogenic aerosols on temperature trends of the sub-thermocline southern Indian Ocean. *Sci. Rep.,* **3,** 2245, doi:10.1038/srep02245.

Delworth, T. L., and K. Dixon, 2006: Have anthropogenic aerosols delayed a greenhouse gas-induced weakening of the North Atlantic thermohaline circulation? *Geophys. Res. Lett.,* **33,** L02606, doi:10.1029/2005GL024980.

——, V. Ramaswamy, and G. Stenchikov, 2005: The impact of aerosols on simulated ocean temperature and heat content in the 20th century. *Geophys. Res. Lett.,* **32,** L24709, doi:10.1029/2005GL024457.

de Szoeke, S. P., S. P. Xie, T. Miyama, K. J. Richards, and R. J. O. Small, 2007: What maintains the SST front north of the eastern Pacific equatorial cold tongue? *J. Climate,* **20,** 2500–2514, doi:10.1175/JCLI4173.1.

Dong, L., T. J. Zhou, and B. Wu, 2014: Indian Ocean warming during 1958–2004 simulated by a climate system model and its mechanism. *Climate Dyn.,* **42,** 203–217, doi:10.1007/s00382-013-1722-z.

Du, Y., and S.-P. Xie, 2008: Role of atmospheric adjustments in the tropical Indian Ocean warming during the 20th century in climate models. *Geophys. Res. Lett.,* **35,** L08712, doi:10.1029/2008GL033631.

Ganguly, D., P. J. Rasch, H. Wang, and J.-H. Yoon, 2012: Climate response of the South Asian monsoon system to anthropogenic aerosols. *J. Geophys. Res.,* **117,** D13209, doi:10.1029/2012JD017508.

Giannini, A., R. Saravanan, and P. Chang, 2003: Oceanic forcing of Sahel rainfall on interannual to interdecadal time scales. *Science,* **302,** 1027–1030, doi:10.1126/science.1089357.

Guemas, V., S. Corti, J. García-Serrano, F. J. Doblas-Reyes, M. Balmaseda, and L. Magnusson, 2013: The Indian Ocean: The region of highest skill worldwide in decadal climate prediction. *J. Climate,* **26,** 726–739, doi:10.1175/JCLI-D-12-00049.1.

Hoerling, M., J. W. Hurrell, T. Xu, G. T. Bates, and A. S. Phillips, 2004: Twentieth century North Atlantic climate change. Part II: Understanding the effect of Indian Ocean warming. *Climate Dyn.,* **23,** 391–405, doi:10.1007/s00382-004-0433-x.

Hong, C.-C., T. Li, LinHo, and Y.-C. Chen, 2010: Asymmetry of the Indian Ocean basinwide SST anomalies: Roles of ENSO and IOD. *J. Climate,* **23,** 3563–3576, doi:10.1175/2010JCLI3320.1.

Jones, G. S., P. A. Stott, and N. Christidis, 2013: Attribution of observed historical near-surface temperature variations to anthropogenic and natural causes using CMIP5 simulations. *J. Geophys. Res.,* **118,** 4001–4024, doi:10.1002/jgrd.50239.

Knutson, T. R., and Coauthors, 2006: Assessment of twentieth-century regional surface temperature trends using the GFDL CM2 coupled models. *J. Climate,* **19,** 1624–1651, doi:10.1175/JCLI3709.1.

Krishnan, R., K. V. Ramesh, B. K. Samala, G. Meyer, J. M. Slingo, and M. J. Fennessy, 2006: Indian Ocean–monsoon coupled interactions and impending monsoon droughts. *Geophys. Res. Lett.,* **33,** L08711, doi:10.1029/2006GL025811.

Lau, K.-M., and H. Weng, 1999: Interannual, decadal–interdecadal, and global warming signals in sea surface temperature during 1955–97. *J. Climate,* **12,** 1257–1267, doi:10.1175/1520-0442(1999)012<1257:IDIAGW>2.0.CO;2.

Lau, N.-C., A. Leetmaa, and M. J. Nath, 2006: Attribution of atmospheric variations in the 1997–2003 period to SST anomalies in the Pacific and Indian Ocean basins. *J. Climate,* **19,** 3607–3627, doi:10.1175/JCLI3813.1.

Lau, W. K. M., M. K. Kim, K. M. Kim, and W. S. Lee, 2010: Enhanced surface warming and accelerated snow melt in the Himalayas and Tibetan Plateau induced by absorbing aerosols. *Environ. Res. Lett.,* **5,** 025204, doi:10.1088/1748-9326/5/2/025204.

Li, T., B. Wang, C. P. Chang, and Y. Zhang, 2003: A theory for the Indian Ocean dipole–zonal mode. *J. Atmos. Sci.,* **60,** 2119–2135, doi:10.1175/1520-0469(2003)060<2119:ATFTIO>2.0.CO;2.

Lohmann, U., and J. Feichter, 2005: Global indirect aerosol effects: A review. *Atmos. Chem. Phys.,* **5,** 715–737, doi:10.5194/acp-5-715-2005.

Lu, J., R. J. Greatbatch, and K. A. Peterson, 2004: Trend in Northern Hemisphere winter atmospheric circulation during the last half of the twentieth century. *J. Climate,* **17,** 3745–3760, doi:10.1175/1520-0442(2004)017<3745:TINHWA>2.0.CO;2.

Meehl, G. A., W. M. Washington, C. M. Ammann, J. M. Arblaster, T. M. L. Wigley, and C. Tebaldi, 2004: Combinations of natural and anthropogenic forcings in twentieth-century climate. *J. Climate,* **17,** 3721–3727, doi:10.1175/1520-0442(2004)017<3721:CONAAF>2.0.CO;2.

Ming, Y., V. Ramaswamy, and G. Chen, 2011: A model investigation of aerosol-induced changes in boreal winter extratropical circulation. *J. Climate,* **24,** 6077–6091, doi:10.1175/2011JCLI4111.1.

Mitchell, J. F. B., T. C. Johns, J. M. Gregory, and S. F. B. Tett, 1995: Climate response to increasing levels of greenhouse gases and sulphate aerosols. *Nature,* **376,** 501–504, doi:10.1038/376501a0.

Pierce, D. W., T. P. Barnett, K. M. AchutaRao, P. J. Glecker, J. M. Gregory, and W. M. Washington, 2006: Anthropogenic warming of the oceans: Observations and model results. *J. Climate,* **19,** 1873–1900, doi:10.1175/JCLI3723.1.

Ramanathan, V., and G. Carmichael, 2008: Global and regional climate changes due to black carbon. *Nat. Geosci.,* **1,** 221–227, doi:10.1038/ngeo156.

Ramaswamy, V., and Coauthors, 2001: Radiative forcing of climate change. *Climate Change 2001: The Scientific Basis,* J. T. Houghton et al., Eds., Cambridge University Press, 349–416.

Rayner, N. A., D. E. Parker, E. B. Horton, C. K. Folland, L. V. Alexander, D. P. Rowell, E. C. Kent, and A. Kaplan, 2003: Global analyses of sea surface temperature, sea ice, and night marine air temperature since the late nineteenth century. *J. Geophys. Res.,* **108,** 4407, doi:10.1029/2002JD002670.

Revelle, R., W. Broecker, H. Craig, C. D. Keeling, and J. Smagorinsky, 1965: Atmospheric carbon dioxide. *Restoring the Quality of Our Environment,* U.S. Government Printing Office, 112–133.

Rotstayn, L. D., M. A. Collier, S. J. Jeffrey, J. Kidston, J. I. Syktus, and K. K. Wong, 2013: Anthropogenic effects on the subtropical jet in the Southern Hemisphere: Aerosols versus long-lived greenhouse gases. *Environ. Res. Lett.,* **8,** 014030, doi:10.1088/1748-9326/8/1/014030.

Sanchez-Gomez, E., C. Cassou, D. L. R. Hodson, N. Keenlyside, Y. Okumura, and T. Zhou, 2008: North Atlantic weather regimes response to Indian–western Pacific Ocean warming: A multi-model study. *Geophys. Res. Lett.,* **35,** L15706, doi:10.1029/2008GL034345.

Schneider, E. K., and M. Z. Fan, 2012: Observed decadal North Atlantic tripole SST variability. Part II: Diagnosis of mechanisms. *J. Atmos. Sci.,* **69,** 51–64, doi:10.1175/JAS-D-11-019.1.

Sen Gupta, A., L. C. Muir, J. N. Brown, S. J. Phipps, P. J. Durack, D. Monselesan, and S. E. Wijffels, 2012: Climate drift in the CMIP3 models. *J. Climate,* **25,** 4621–4640, doi:10.1175/JCLI-D-11-00312.1.

Sigmond, M., M. C. Reader, J. C. Fyfe, and N. P. Gillett, 2011: Drivers of past and future Southern Ocean change: Stratospheric ozone versus greenhouse gas impacts. *Geophys. Res. Lett.,* **38,** L12601, doi:10.1029/2011GL047120.

Smith, T. M., and Coauthors, 2008: Improvements to NOAA's historical merged land–ocean surface temperature analysis (1880–2006). *J. Climate,* **21,** 2283–2296, doi:10.1175/2007JCLI2100.1.

Solomon, S., D. Qin, M. Manning, Z. Chen, M. Marquis, K. Averyt, M. Tignor, and H. L. Miller Jr., Eds., 2007: *Climate Change 2007: The Physical Science Basis.* Cambridge University Press, 996 pp.

Song, F., T. Zhou, and Y. Qian, 2014: Responses of East Asian summer monsoon to natural and anthropogenic forcings in the 17 latest CMIP5 models. *Geophys. Res. Lett.,* **41,** 596–603, doi:10.1002/2013GL058705.

Stowasser, M., H. Annamalai, and J. Hafner, 2009: Response of the South Asian summer monsoon to global warming: Mean and synoptic systems. *J. Climate,* **22,** 1014–1036, doi:10.1175/2008JCLI2218.1.

Taylor, K. E., R. J. Stouffer, and G. A. Meehl, 2012: An overview of CMIP5 and the experiment design. *Bull. Amer. Meteor. Soc.,* **93,** 485–498, doi:10.1175/BAMS-D-11-00094.1.

Trenary, L. L., and W. Han, 2013: Local and remote forcing of decadal sea level and thermocline depth variability in the south Indian Ocean. *J. Geophys. Res.,* **118,** 381–398, doi:10.1029/2012JC008317.

Vecchi, G. A., and B. J. Soden, 2007: Global warming and the weakening of the tropical circulation. *J. Climate,* **20,** 4316–4340, doi:10.1175/JCLI4258.1.

Wilks, D. S., 1995: *Statistical Methods in the Atmospheric Sciences.* Academic Press, 467 pp.

Xie, S.-P., C. Deser, G. A. Vecchi, J. Ma, H. Y. Teng, and A. T. Wittenberg, 2010: Global warming pattern formation: Sea surface temperature and rainfall. *J. Climate,* **23,** 966–986, doi:10.1175/2009JCLI3329.1.

——, B. Lu, and B. Xiang, 2013: Similar spatial patterns of climate responses to aerosol and greenhouse gas changes. *Nat. Geosci.,* **6,** 828–832, doi:10.1038/ngeo1931.

Zheng, X.-T., S.-P. Xie, G. A. Vecchi, Q. Liu, and J. Hafner, 2010: Indian Ocean dipole response to global warming: Analysis of ocean–atmospheric feedbacks in a coupled model. *J. Climate,* **23,** 1240–1253, doi:10.1175/2009JCLI3326.1.

——, ——, Y. Du, L. Liu, G. Huang, and Q. Liu, 2013: Indian Ocean dipole response to global warming in the CMIP5 multimodel ensemble. *J. Climate,* **26,** 6067–6080, doi:10.1175/JCLI-D-12-00638.1.

Zhou, T., and Coauthors, 2009: Why the western Pacific subtropical high has extended westward since the late 1970s. *J. Climate,* **22,** 2199–2215, doi:10.1175/2008JCLI2527.1.